International Journal of Research Publication and Reviews

Investigation of the Aerodynamic Characteristics of Aircraft Propellers Using Unsteady Nonlinear Vortex-Lattice Method

MSc The Son Nguyen [a], Ph. D Truong Thanh Nguyen [b]

Air Force Officer's College [a,b] , Nha Trang City, Khanh Hoa, 650000, Vietnam

A B S T R A C T

This paper presents an investigation of computational model to calculate propeller characteristics by unsteady nonlinear vortex-lattice method, creating the algorithms and a program, thereby assessing the impact of certain factors on the propeller characteristics. The paper also introduces the results: The dependence of the propeller characteristics (thrust coefficient, thrust, and useful power on the propeller) on the rotation speed, flight conditions (V, H) and the propeller's geometrical characteristics (number of blades, radius, blade's chord, blade installation angle). The results accurately reflect the physics of the nonstop flow interacting with propeller. This algorithm can be used to calculate the properties of the propeller in the process of designing propellers with the given flight characteristics

Keywords: Uhs: Vortex-lattice method; Aerodynamic characteristics of aircraft propellers; Theory of non-stationary discrete vortex.

1. Introduction

In all aerodynamics problems, once the shape and motion laws of an aircraft's wings or propellers in particular are known, the problem can be defined as determining the characteristic parameters of the flow around the blades (such as velocity and pressure) and its aerodynamic characteristics.

For blades, one of the requirements is to ensure a high level of thrust, power, and efficiency at the given altitude and airspeed.

The problem is defined as a model of a propeller blade with a given geometrical size, being rotated by a motor with a speed of n (revolutions per minute), causing the propeller blade to move at a velocity of V, at an angle of attack α (the angle formed by the rotation axis of the propeller blade and the velocity of the airflow).

As the propeller blade rotates and translates, the airflow around the propeller blade will exert a force on the surface of the propeller blade, creating thrust and generates useful work on the propeller blade.

These characteristics will change as the dynamic and geometric parameters change. The problem determines the propeller blade characteristics: the propeller blade characteristics with respect to engine speed, airspeed, and altitude; the propeller blade characteristics when changing the propeller blade radius, number of propeller blades, blade chord, and blade installation angle. The authors have used a unsteady nonlinear vortex-lattice method for calculating the aerodynamic characteristics of an aircraft propeller blade.

2. The calculation model

2.1. Assumptions

The flow around the object is an ideal gas environment, incompressible, not viscous, and does not take into account the thickness of the force-generating surface.

Outside the blade, the law of conservation of mass and the continuity equation are satisfied.

On the vortex sheet behind and on both sides of the propeller blade, the condition for continuity pressure is satisfied, that is, the vortex sheet moves with the environment. At a distance far enough from the propeller blade and its trace, the disturbances can be eliminated, and the flow becomes non-disturbed. The shape of the propeller blade remains unchanged when participating in rotational and translational motion.

2.2. Coordinate systems.

The fixed on the blades coordinate system $O_1x_1y_1z_1$ has O_1 located at the center of the propeller, the direction of the undisturbed airflow velocity V coincides with O_1x_1 at an angle α_{cq}, O_1y_1 is perpendicular to O_1x_1 and lies in the plane of rotation of the blade. O_1z_1 is perpendicular to $O_1x_1y_1$ and forms a right-handed coordinate system.

The second coordinate system is the propeller-fixed coordinate system $O_1x_{cq}y_{cq}z_{cq}$ with O_1 located at the center of the propeller, $O_1x_{cq} \equiv O_1x_1$, O_1y_{cq} is perpendicular to O_1x_1 and lies in the plane of the blade (Figure 1, 2).

The nondimensional coordinates of any point of $O_1x_1y_1z_1$ are denoted ξ, η, ς by $\xi = \frac{x_1}{R}; \eta = \frac{y_1}{R}; \varsigma = \frac{z_1}{R}$.   (2.1)
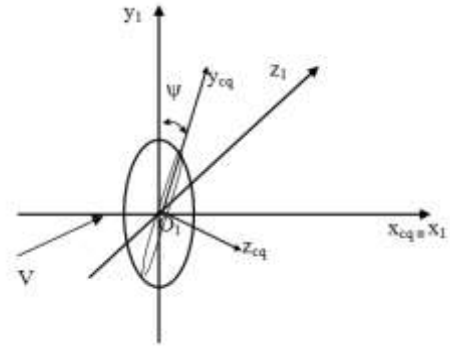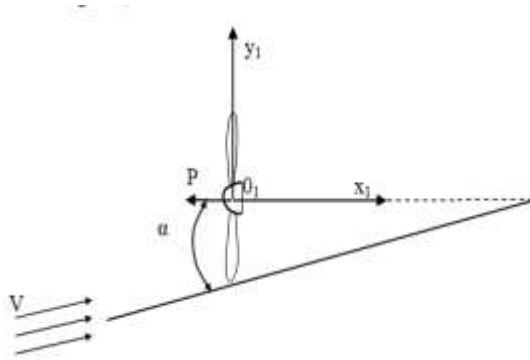
Figure 1. Computational model of aerodynamic characteristics of the blades   Figure 2. Coordinate system of the blades

2.3. Propeller Blade Modeling Using Vortex Sheet

The model is constructed using the non-linear discrete vortex method considering in continuous flow and is considered in a flight condition in an ideal gas flow. According to the discrete vortex method, the blade is divided into elements and replaced by vortex sheet (vortices in the coordinate system $O_1x_1y_1z_1$). The vortex sheet, that replaces the propeller blade, is the vortex sheet on the blades and free vortices outside the blades (zone I_1 flows out of the trailing edge of the blade; zone II_1 flows out of the inner part of the blade, region III_1 flows out of the outer part of the blade (Figure 3). Measurement points are arranged on the propeller blade and must satisfy the Chaplygin–Zhukovsky hypothesis at the blade edge and satisfy the impermeable boundary condition on the blade surface.

2.4. Determination of the induced velocity field downstream of the propeller blade

When replacing the load-bearing surface of the propeller blade with a system of discrete vortices, the chord of each blade section is divided into n_1 parts, and the span of the blade is divided into N_1 strips (parts) (Figure 3). The horizontal vortices are denoted by μ_1 with the initial point at the leading edge of the blade. The horizontal vortices of the blade are numbered according to ($1 \le \mu_1 \le n_1$), the horizontal vortices of region I $\left(n_1 + 1 \le \mu_1 \le n_1 + r\right)$.

To determine the induced velocity caused by the vortex system of the blade at any point in its vicinity, we need to know the intensity of the vortices on the vortex plane at time r and the induced velocity of the unit vortex at that point.

From the above problem in the article, we will determine the induced velocity at two positions: the test points and the end points of the vortex sheet.
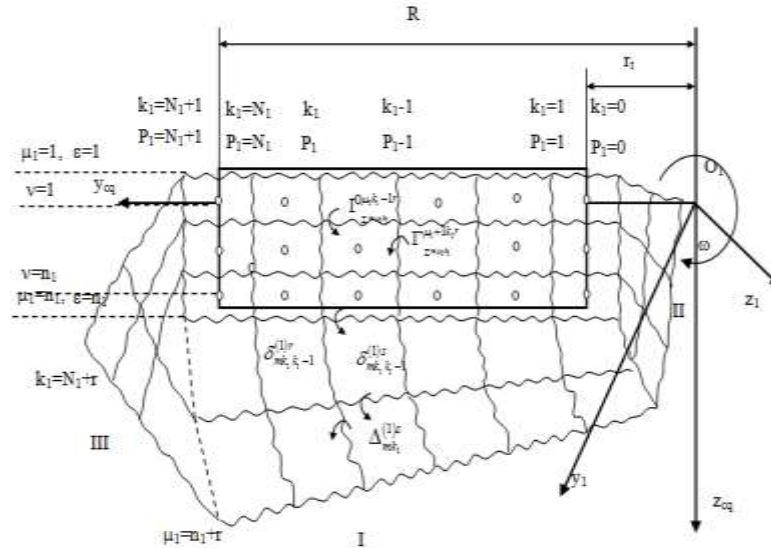
Figure 3. Schematic of vortex sheet replacing blades.

Setting up the equation system to determine the vortex strength.

From the impermeable boundary condition on the blade surface, which means the induced velocity caused by the vortex at the test points must be zero at the first iteration when $\tau=0$, and at the next iteration, the induced velocity at the test points must be equal to the induced velocity at the previous iteration. Combining this with the conservation of the circulation of the velocity around any closed contour, we have the following system of equations:

$$\sum_{m=1}^{k_{lc}}\sum_{k_1=1}^{N_1+1}\sum_{\mu_1=1}^{n_1}\Gamma_{\Sigma m\mu_1 k_1}^{\mu_1 k_1-1r}a_{m\mu_1 k_1 0v}^{\mu_1 k_1-1p_1 p_1-1}+\sum_{m=1}^{k_{lc}}\sum_{k=1}^{N_1+1}\delta_{mk_1 k_1-1}^{(1)s}a_{mn_1+1k_1 0v}^{n_1+1k_1-1p_1 p_1-1}=H_{m0v}^{p_1 p_1-1}$$

$$\sum_{\mu_1=1}^{n_1}\Gamma_{\Sigma m\mu_1 k_1}^{\mu_1 k_1-1r}+\delta_{mk_1 k_1-1}^{(1)s}=-\sum_{s=1}^{r-1}\delta_{mk_1 k_1-1}^{(1)s} \tag{2.2}$$

The coefficients on the left-hand side of the system of equations are expressed as non-dimensional functions as follows:

$$a_{m\mu_1 k_1 0v}^{\mu_1 k_1-1p_1 p_1-1}=\frac{1}{4\pi}\Bigg\{\Bigg[v_{m\mu_1 k_1 0vx_1}^{\mu_1 k_1-1p_1 p_1-1}+\sum_{\varepsilon=\mu_1}^{n_1}\left(v_{m\varepsilon k_1-10vx_1}^{\varepsilon+1k_1-1p_1 p_1-1}-v_{m\varepsilon k_1 0vx_1}^{\varepsilon+1k_1 p_1 p_1-1}\right)\Bigg]cos(n_{0v}^{p_1 p_1-1},x_1)+$$

$$+\Bigg[v_{m\mu_1 k_1 0vy_1}^{\mu_1 k_1-1p_1 p_1-1}+\sum_{\varepsilon=\mu_1}^{n_1}\left(v_{m\varepsilon k_1-10vy_1}^{\varepsilon+1k_1-1p_1 p_1-1}-v_{m\varepsilon k_1 0vy_1}^{\varepsilon+1k_1 p_1 p_1-1}\right)\Bigg]cos(n_{0v}^{p_1 p_1-1},y_1)+$$

$$+\Big[v_{m\mu_1 k_1 0vz_1}^{\mu_1 k_1-1p_1 p_1-1}+\sum_{\varepsilon=\mu_1}^{n_1}\left(v_{m\varepsilon k_1-10vz_1}^{\varepsilon+1k_1-1p_1 p_1-1}-v_{m\varepsilon k_1 0vz_1}^{\varepsilon+1k_1 p_1 p_1-1}\right)\Big]cos(n_{0v}^{p_1 p_1-1},z_1)\Big\} \tag{2.3}$$

$$a_{mn_1+1k_1 0v}^{n_1+1k_1-1p_1 p_1-1}=\frac{1}{4\pi}\Big[v_{mn_1+1k_1 0vx_1}^{n_1+1k_1-1p_1 p_1-1}cos(n_{0v}^{p_1 p_1-1},x_1)+v_{mn_1+1k_1 0vy_1}^{n_1+1k_1-1p_1 p_1-1}cos(n_{0v}^{p_1 p_1-1},y_1)+$$

$$+v_{mn_1+1k_1 0vz_1}^{n_1+1k_1-1p_1 p_1-1}cos(n_{0v}^{p_1 p_1-1},z_1)\Big] \tag{2.4}$$

$$H_{m0v}^{p_1 p_1-1}=H_1+H_2+H_3 \tag{2.5}$$

Where $H_{m0v}^{p_1 p_1-1}$- is the total velocity along the tangent to the blade surface (at the measurement points) of the non-disturbed flow (including the translational motion and rotational motion of the blade) and the induced velocity caused by the vortex at the previous time step.

The corresponding components H_1, H_2, H_3 are determined as follows:

$$H_1=\left[-v\,cos\alpha_{cq}\,cos\psi+\left(1+\overline{\omega}_y\right)\varsigma_{0v}^{p_1 p_1-1}+\overline{\omega}_z\eta_{0v}^{p_1 p_1-1}-H_x\right]cos(n_{0v}^{p_1 p_1-1},x_1)$$

$$H_2=\left[-v\,cos\alpha_{cq}-\left(\overline{\omega}_z\xi_{0v}^{p_1 p_1-1}-\overline{\omega}_x\varsigma_{0v}^{p_1 p_1-1}\right)-H_y\right]cos(n_{0v}^{p_1 p_1-1},y_1)$$

$$H_3=\left[-v\,cos\alpha_{cq}\,sin\psi+\left(1+\overline{\omega}_y\right)\xi_{0v}^{p_1 p_1-1}+\overline{\omega}_x\eta_{0v}^{p_1 p_1-1}-H_z\right]cos(n_{0v}^{p_1 p_1-1},z_1) \tag{2.6}$$

The components of induced velocity H_j in formula (2.6) at the previous time steps are:

$$H_j=\frac{1}{4\pi}\sum_{m=1}^{k_{lc}}\sum_{s=1}^{r-1}\Bigg[\sum_{k_1=1}^{N_1+1}\delta_{mk_1 k_1-1}^{(1)s}v_{mn_1+r-s+1k_1 0vj}^{n_1+r-s+1k_1-1p_1 p_1-1}+\sum_{k_1=1}^{N_1}\Delta_{mk_1}^{(1)s+1}v_{mn_1+r-s+1k_1 0vj}^{n_1+r-s+1k_1 p_1 p_1-1}+$$

$$+\sum_{\mu_1=1}^{n_1}\delta_{m\mu_1\mu_1+1}^{(2)s}v_{m\mu_1 N_1+r-s-10vj}^{\mu_1+1N_1+r-s+1p_1 p_1-1}+\sum_{\mu_1=1}^{n_1}\Delta_{m\mu_1}^{(2)s+1}v_{m\mu_1 s-r+10vj}^{\mu_1 N_1+r-s+1p_1 p_1-1}+$$

$$+ \sum_{\mu_1=1}^{n_1} \delta_{m\mu_1\mu_1+1}^{(3)s} v_{m\mu_1 N_1+r-s+10vj}^{\mu_1+1N+r-s+1p_1p_1-1} + \sum_{\mu_1=1}^{n_1} \Delta_{m\mu_1}^{(3)s+1} v_{m\mu_1 N_1+r-s0vj}^{\mu_1+1N+r-s+1p_1p_1-1} \Bigg] +$$

$$- \frac{1}{4\pi} \sum_{m=1}^{k_{lc}} \left(\sum_{\mu_1=1}^{n} \Gamma_{\Sigma m\mu_1 1}^{\mu 0r-1} v_{m\varepsilon 00vj}^{\varepsilon+10p_1p_1-1} + \sum_{\varepsilon=\mu_1}^{n} \Gamma_{\Sigma m\mu_1 N_1+1}^{N_1 r-1} v_{m\varepsilon N_1+10vj}^{\varepsilon+1N_1+1_1p_1p_1-1} \right) \qquad (j=(x_1,y_1,z_1)) \qquad (2.7)$$

2.5. Determining aerodynamic characteristics

To determine the aerodynamic characteristics of the propeller, we must determine the pressure difference on the blade surface when the propeller rotates with speed ω, flying with speed v, at the check points. Considering the case of the propeller propeller model under study, from the geometrical relationship (Figure 4) can be determined:

$$v_{00t} = \left(v_{x0}\sin\psi_L + v_{z0}\cos\psi_L\right)\cos\varphi - v_{y0}\sin\varphi; \qquad v_{00t} = v_{x0}\cos\psi_L - v_{z0}\sin\psi_L \qquad (2.8)$$

The differential is rewritten:

$$\Delta\bar{p} = 2\left\{\left[\left(v_{x0}\sin\psi_L + v_{z0}\cos\psi_L\right)\cos\varphi_0 - v_{y0}\sin\varphi_0\right]\gamma_{\Sigma} - \left(v_{x0}\cos\psi_L - v_{z0}\sin\psi_L\right)\gamma_{\Sigma} - \frac{\partial\Gamma_L}{\partial\tau}\right\} \qquad (2.9)$$
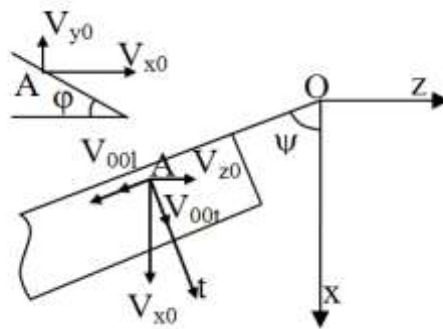
$$v_{x0} = v_{xt} - u_0\cos\alpha\cos\psi_L - \left[\left(1-\bar{\omega}_y\right)\bar{z} - \bar{\omega}_z\bar{y}\right]$$

$$v_{y0} = v_{yt} - u_0\sin\alpha - \left(\bar{\omega}_z\bar{x} - \bar{\omega}_x\bar{\omega}_z\right)$$

$$v_{z0} = v_{zt} - u_0\cos\alpha\sin\psi_L - \left[\bar{\omega}_x\bar{y} - \left(1-\bar{\omega}_y\right)\bar{x}\right]$$

v_{x0}, v_{y0}, v_{z0} - dimensionless relative velocity;

v_{xa}, v_{ya}, v_{za} - dimensionless absolute velocity; α is the angle between the initial current and the axis of rotation of the propeller.

Figure 4. Geometrical relationships for determining theload on the blade.

From the vortex intensity determined from solving the system of equations (2.2), using the Cosi-Lagrangian integral (2.9), we can determine the aerodynamic load acting on the surface of the blade of the propeller with the form:

$$\Delta\bar{p} = 2\left\{\left[\left(v_{0x1}\sin\psi_L + v_{0z1}\cos\psi_L\right)\cos\varphi - v_{0y1}\sin\varphi\right]\gamma_{\Sigma\varphi1}^{\varepsilon p_1-1r} - \left(v_{0x1}\cos\psi_L - v_{0z1}\sin\psi_L\right)\gamma_{\Sigma m\varphi_1 L}^{\varepsilon+1p_1-1r} - \frac{\partial\Gamma_{\varepsilon p_1 L}^{\varepsilon p_1-1r}}{\partial\tau}\right\} \qquad (2.10)$$

In there:- $v_{0x_1}, v_{0y_1}, v_{0z_1}$ is the velocity along the axes O_1x_1, O_1y_1, O_1z_1 of the midpoint of the spin; ψ_L - horizontal bevel; - $\gamma_{\Sigma x\varphi1}^{\varepsilon p_1-1r}$ Dimensionless intensity of the vortex distribution layer;

$\gamma_{\Sigma x\varphi1}^{\varepsilon p_1-1r}$ expressed through discrete vortex velocities according to the formulas:

$$\gamma_{\Sigma\varphi1}^{\varepsilon p_1-1r} = \Gamma_{\Sigma\varphi1}^{\varepsilon p_1-1r} \frac{n}{\bar{b}_{\varphi_1 p_1-1}} \frac{1}{\cos\chi_{\Sigma\varphi_1}^{\varepsilon p_1-1r}} \qquad (2.11)$$

$$\gamma_{\Sigma\varepsilon1 t\varphi1}^{\varepsilon p_1-1r} = \Gamma_{\Sigma\varepsilon1t\varphi1}^{\varepsilon+1p_1-1r} \frac{1}{\ell_{p_1 p_1-1}}$$

Velocity of internal longitudinal vortex $\bar{l}_{\Sigma\varepsilon1 t\varphi}^{\varepsilon+1p_1-1r}$ (3.11)counted:

$$\Gamma_{\Sigma\kappa e-1\rho_1}^{\kappa+1\rho_1-1r} = \frac{1}{4}\left(\Gamma_{\Sigma\kappa e-1\rho_1}^{\kappa e r} + \Gamma_{\Sigma\kappa e\rho_1}^{\kappa+1\rho_1 r} + \Gamma_{\Sigma\kappa e-1\rho_1-1}^{\kappa e\rho_1-1r} + \Gamma_{\Sigma\kappa e\rho_1-1}^{\kappa+1\rho_1-1r}\right) \tag{2.12}$$

The change in total velocity along the cyclic *L* is the result of the emergence and exit of the impeller blades of free vortexes, thus:

$$\Delta\Gamma_{\Sigma\omega\iota\iota}^{\kappa\rho_1-1\iota} = \sum_{\mu_1=\kappa}^{n_1}\left(\Gamma_{\Sigma\mu\rho_1}^{\mu_1\rho_1-1r} - \Gamma_{\Sigma\kappa\rho_1}^{\mu_1\rho_1-1r-1}\right) + \delta_{\rho_1\rho_1-1}^{(1)r} \tag{2.13}$$

Cyclic velocity change *L* happened in the time $\Delta\tau$ period. When the time step is small enough, it can be considered:

$$\frac{\partial\Gamma_{c_1,L}^{\kappa\rho_1-1r}}{\partial\tau} \approx \frac{\Delta\Gamma_{c_1,L}^{\kappa\rho_1-1r}}{\Delta\tau} \tag{2.14}$$

After determining the aerodynamic load on the blade surface, the integral for all the computational cells will determine the force acting on the sections and from here determine the force acting on the blades and the blade's thrust coefficient can be determined.

$$C_{y\kappa\rho_1}^{\rho_1\ 1r} = \frac{1}{n_1}\sum_{r=2}^{N_1}\Delta P_{\kappa\kappa\rho_1}^{\kappa\rho_1\ 1r} \tag{2.15}$$

$$C_T^r = \frac{1}{\pi N_1}\left(\sum_{\kappa=1}^{k_1}\sum_{\rho_1=2}^{N_1}C_{y\kappa\rho_1}^{\rho_1-1r}\cos\varphi_{\kappa\rho_1}^{\rho_1-1r} + \frac{1}{2}C_{y\kappa 1}^{0r}\cos\varphi_{\kappa 1}^{0r} + \frac{1}{2}C_{y\kappa N_1+1}^{N_1r}\cos\varphi_{\kappa N_1+1}^{N_1r}\right)\overline{b}$$

The thrust force is determined:

$$P = C_t^r\frac{\rho V^2}{2}S_1 \tag{2.16}$$

The useful power of propeller: $N_{cq} = P.V$ (2.17)

In Equation (2.15), the aerodynamic characteristic coefficients of aircraft propellers are determined. This aerodynamic coefficient at each value of angle of attack α depends on the intensity of the vortex; at different angles of attack will depend on different spins. From there, the thrust coefficient (aerodynamic force) C_T is a quantity that is nonlinearly dependent on the angle of attack α.

The time step to investigate the blade characteristics under the influence of the propeller is: τ1/Δτ.

3. Results

3.1. Results according to the rotation characteristic

Engine working in rotation mode n = 0÷6000 v/min; A given airspeed V = 50m/s; altitude H = 1000 m; angle of attack α = 0 (angle combined by propeller shaft and airspeed); Defined propeller geometry parameters (Number of blades: 2; Outer radius R = 1.2m; Inner radius r = 0.27m; Blade chord b = 0.21m; Installation angle ϕ = 30⁰ at the cross section r = 0.75.R).
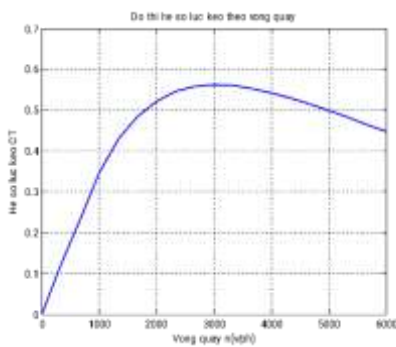

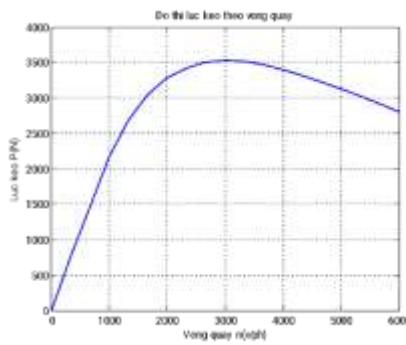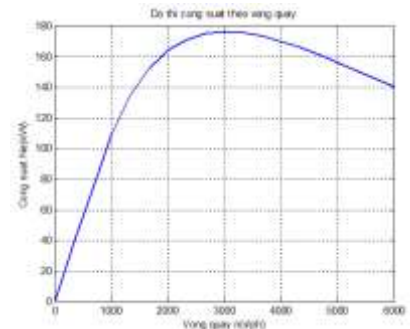**Figure 5. Thrust coefficient**
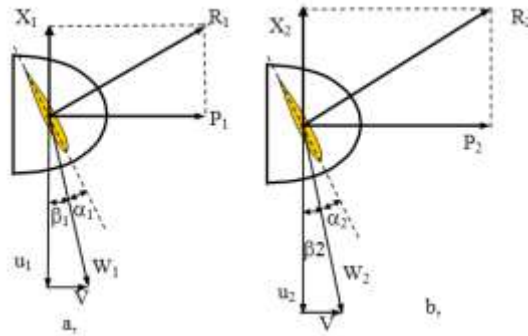
Figure 6. Thrust Force

Figure 7. Useful power

Figure 8. The influence of rotation

As the blade rotation speed increases, the axial velocity u (Figure 8) on the blade increases ($u_2 > u_1$), while V = const, the total velocity W on the blades increases ($W_2 > W_1$). On the other hand, as u increases, the angle of entry β decreases, while the mounting angle stays the same, so the angle of attack on the blade $α_1$ increases (α = φ -β) when the angle of attack on the blade increases, the synthesis speed W increases, the thrust coefficient increases, the thrust force, the useful power on the propeller increases and reaches the maximum. When the rotation n continues to increase, the angle of attack on the blade has a large value, causing current separation on the blade, so the coefficient of thrust and thrust decreases, so the effective power of the propeller decreases.

3.2. Result of propeller characteristics in flight mode

3.2.1. Result of propeller characteristics at different airspeeds

Keeping the calculated parameters unchanged, change the flight speed by V = 0÷160 m/s, and the lift coefficient, lift force, and useful power of the blades are investigated as a function of airspeed, as shown in Figures 9, 10, and 11.
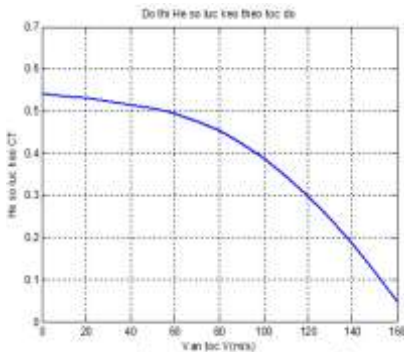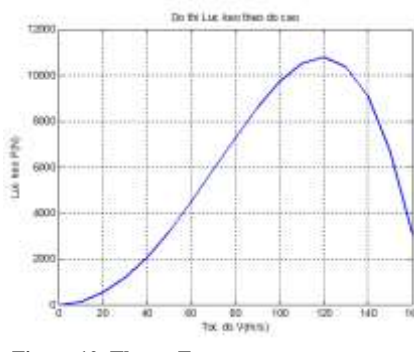

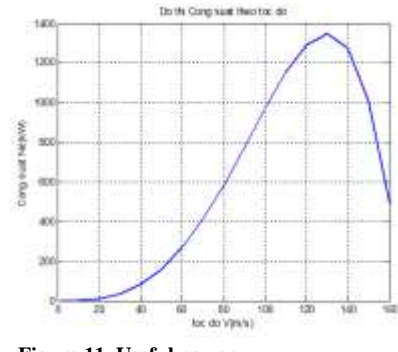**Figure 9. Thrust coefficient**

Figure 10. Thrust Force

Figure 11. Useful power

According to the airspeed, the thrust coefficient decreases with increasing speed (Figure 9). As the speed V increases, the rotation n remains constant, so β increases, while the installation angle remains constant so the angle of attack on the blade $α_1$ gradually decreases leading to a decrease in the propeller thrust coefficient.
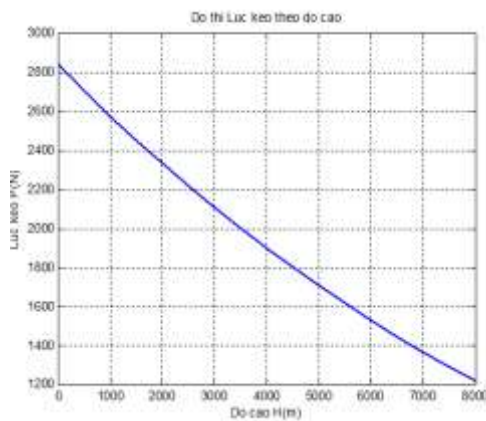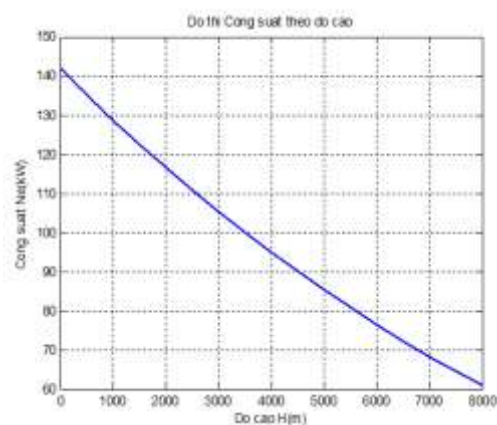

Figure 12. Thrust Force

Figure 13. Useful power

The propeller thrust force is determined by the formula. $P = C_T \frac{\rho v^2}{2} S_c$ Although the thrust coefficient decreased, the propeller thrust increased in the range V = 0÷120m/s because the increase in speed squared was greater than the decrease in the thrust coefficient. When V> 120 m/s, the decrease in thrust coefficient is larger than the squared increase in speed, so the thrust decreases (Figure 10).

3.2.2. Result of propeller characteristics according to flight altitude

Change the altitude H = 0 ÷ 8000 m, while maintaining the calculation parameters. The thrust coefficient $C_T = 0.5218$ is obtained from the graph in Figure 5, the thrust force, and useful power of the blade according to airspeed are determined using formulas (2.16) and (2.17) and presented in Figures 12 and 13. When the altitude changes, air density ρ decreases, so thrust, propeller power decrease.

3.3. Calculation results of propeller characteristics based on geometric characteristics

3.3.1. Propeller characteristic results when changing the number of leaves

With the parameters of the engine and the geometric parameters given above, the results were obtained for different numbers of blades:

The thrust coefficient C_T of propellers 2, 3, 4, 5, 6 blades respectively: 0.5005; 0.7208; 0.8626; 0.3356; 0.1040.

The thrust force P (N) of propellers 2, 3, 4, 5, 6 blades respectively: 3141.5; 4524.4; 5414.3; 2106.4; 653.0.

Power (kW) of propellers 2, 3, 4, 5, 6 blades respectively: 157.0732; 226.2196; 270.7165; 105.3201; 32.6524.

When the number of blades increases from 2 to 4, the thrust coefficient, thrust force, and useful power of the propeller increase. When the number of blades increases to 5 or 6, the dynamic interference between the blades increases, leading to a sharp increase in the resistance torque, resulting in a decrease in thrust coefficient, thrust force, and useful power of the blade.

3.3.2. Calculation results of propeller characteristics when changing radius

The dependence of thrust coefficient, thrust force, and useful power of the fan on the radius of the fan was studied in the range of outer radius R = 0.27 - 2 (m). The results are shown in Figures 14, 15, 16.

The thrust coefficient increases as the blade radius increases (Figure 14) because when the installation angle is constant, the angle of entry decreases (), so the angle of attack on the blade increases (α = φ -β).

$$\beta = \text{arctg}\left(\frac{V}{\omega r}\right)$$

At small radius values R = 0.27 ÷ 0.7 m, the rate of increase is slow, because at this time, the leaf area is small, so the load is applied to the small blade. When the radius is large enough (R = 0.8 ÷1.6 m), the area of the blade is large, so the thrust coefficient increases rapidly (Figure 14).

The rotor radius increases (R = 0.27 ÷ 1.6 m), the rotational plane area increases, and the thrust coefficient and thrust force of the fan increase, leading to an increase in useful power.

When R > 1.6m, the decrease in thrust coefficient is greater than the increase in the area of the rotating plane, resulting in a decrease in thrust force and useful power of the fan (Figures 15, 16).
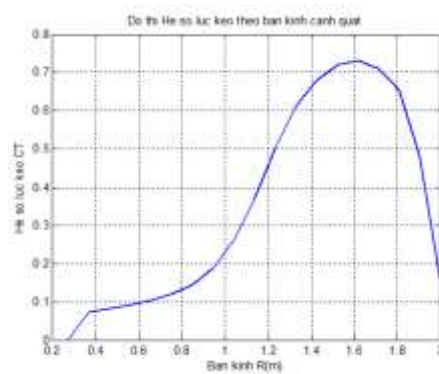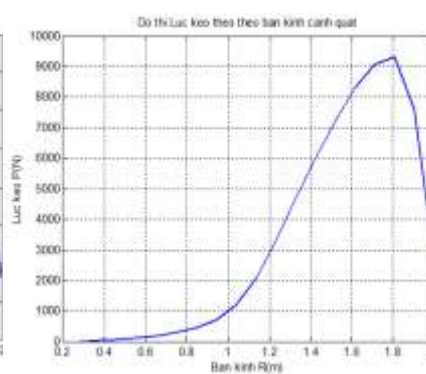

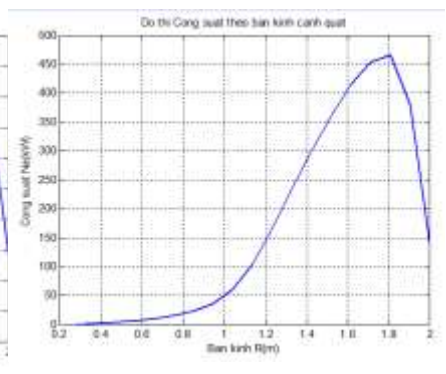**Figure 14. Thrust coefficient**   **Figure 15. Thrust Force**   **Figure 16. Useful power**

3.3.3. Characteristic results when changing blade arc width

Change the magnitude of the chord, while keeping the computational parameters constant. On the Figures 17, 18, 19 are the results showing the relationship between the blade chords and the coefficient of thrust , thrust and useful power of the propeller.
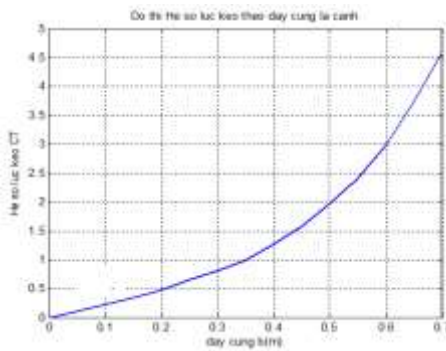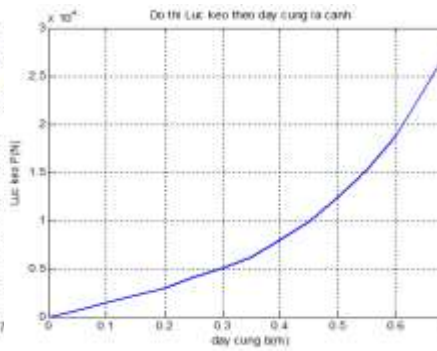
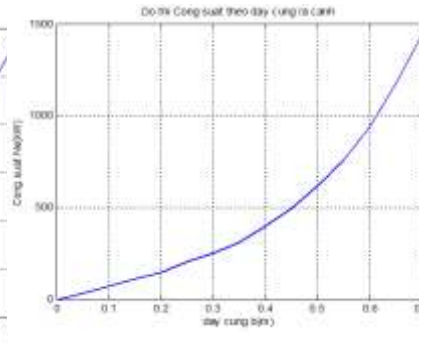**Figure 17. Thrust coefficient**   **Figure 18. Thrust Force**   **Figure 19. Useful power**

When the propeller rotation is constant, the flight speed is constant, the blade chord increases, leading to an increase in the blade area, so the thrust coefficient increases (Figure 17), the thrust increases (Figure 18) and useful power of the blade increases (Figure 19). Since the thrust coefficient increases proportionally to the blade chord, and the mesh of the calculation is the same, the increase of these quantities is larger (faster) to the right of the graph (when the chord is propeller increases).

Due to the rapid increase in the thrust coefficient, the thrust force is large when the blade's bowstring increases, so the useful power generated on the propeller is very large. However, to have a large power on the propeller, the engine power needs to be large, on the other hand, when the blade has a large width, the rotational resistance torque will be large, so the larger the engine power, the better. reduce the efficiency of the propeller.

3.3.4. Characteristic of the blade at different installation angles

With the change in blade installation angle, the thrust coefficient, thrust force and useful propeller power are shown on the graphs Figure 20, 21, 22.

When installation angle increases in the range of $0 \div 30^0$ (at the cross-section r = 0.75.R) the angle of entry β remains constant, so the blade angle of attack α_l increase leads to an increase in the coefficient of thrust, traction and useful propeller power. In places where the blades are too small, the angle of attack α of the blades is too small, the thrust force of the blades is very small, and the useful power of the blades is also very small. At this time, most of the useful power of the engine is consumed by the frictional resistance between the blade and the air. When mounting angle $> 30^0$ the blade angle of attack increases too much, leading to the separation of current on the blade, increasing the thrust torque, reducing the thrust force, reducing the useful work of the propeller, the useful work of the engine is consumed by the thrust.
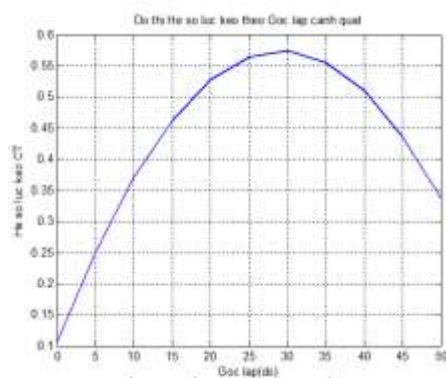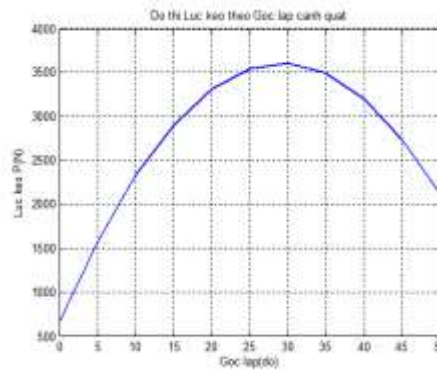
Figure 20. Thrust coefficient   **Figure 21. Thrust Force**   **Figure 22. Useful power**

In order to ensure no separation of current on the blades, in the sections according to the radius of the angle of attack, the leaf is close to the beneficial angle of attack, so now the mounting angle at the sections is determined according to the favorable angle of attack. given airspeed, angular velocity, and propeller radius. The value of$_{profit}$ depends on the forward ratio λ. When the forward ratio is small, the mounting angle$_{cl}$ will be small, but the leaf angle of attack is still guaranteed at a beneficial angle of attack, the rotational resistance is small, so the propeller performance is ensured. Or when the forward ratio is relatively large, the mounting angle$_{cl}$ big.

CONCLUSION

 On the basis of applying the theory of non-stationary discrete vortex, the authors have modeled and built an algorithm and a solution program to determine the aerodynamic characteristics of aircraft propellers. The authors have built a method to determine the induced speed generated by the aircraft propeller in the space adjacent to the propeller and the propeller characteristics. Calculation results accurately reflect the physical and reliable nature of the non-stop flow interacting with the operation of the impeller. These results can be used to investigate the propeller characteristics in the process of calculating the propeller design for the aircraft. With the determination of the induced speed generated by the aircraft propeller in the space adjacent to it, the software can be extended to calculate the propeller's interaction effect on other aircraft components as well as with the limiting face.

References

[1]   Vu Ngoc Hoe (2011). *Aerodynamics*. Air Defense Academy, Hanoi.

[2]   Hartman E.P., Biermann D (1938), "The aerodynamic characteristics of full scale propellers having 2,

[3]   3 and 4 blades of Clark Y and RA.F airfoil sections", *Technical report No. 640*, NACA.

[4]   Burago S.G., Kushalov A.N. (1985). *Aerodynamic calculation of an aircraft propeller*, published by MAI, Moscow.